Enhanced Infusion of Gold Nanocrystals into Mesoporous Silica with Supercritical Carbon Dioxide

Gaurav Gupta, Parag S. Shah, Xiaogang Zhang, Aaron E. Saunders, Brian A. Korgel, and Keith P. Johnston*

Department of Chemical Engineering and Texas Materials Institute, Center for Nano- and Molecular Science and Technology, The University of Texas, Austin, Texas 78712-1062

Received May 17, 2005. Revised Manuscript Received August 15, 2005

Gold nanocrystal dispersions in toluene−CO_2 mixtures were infused into cylindrical pores in mesoporous silica to achieve high loadings over 2 wt % in 24 h. The nanocrystals were highly dispersed according to transmission electron microscopy, and the loadings approached equilibrium. In contrast, the loadings were small for infusion with pure toluene or toluene mixed with an antisolvent, methanol. The differences in loading were correlated with the long-ranged van der Waals forces between gold and silica through the intervening solvent. These van der Waals forces became stronger as CO_2 was added to toluene, as a consequence of a reduction in the Hamaker constant of the mixed intervening solvent, resulting in stronger nanocrystal adsorption. The decoupling of the nanocrystal synthesis step and the infusion step leads to exquisite control of the nanocrystal size, morphology, and dispersibility within the pores. The simplicity of the method allows for the facile production of nanocrystal/silica composites for applications such as catalysis and optoelectronics.

Introduction

Decreasing the size of metals and semiconductors leads to unique size-dependent electronic, optical, and catalytic properties, which deviate from the bulk.[1−4] One of the key challenges is to control the arrangement of nanocrystals in various substrates including block copolymer patterned templates,[5] nanoscale features patterned by e-beam lithography,[6] and nanoporous materials[7] as described in Table 1. Reactive precursors may be deposited into a porous material from either the gas phase or via a wetting liquid in order to synthesize nanocrystals within the pores.[8−13] Here, the size and the shape of the pores may be used as a template to control the particle size and shape and to form spherical particles[10] or, in the case of cylindrical pores, nanowires.[9,11,12,14] The diffusion of precursors and nanocrystals through the solvent may be undesirably slow for mesopores. It took about 3 weeks for $HAuCl_4$ aqueous precursor solution to completely infiltrate mesoporous silica,[13] perhaps indicating diffusional resistances of entrapped air in regions of variable curvature.[15]

Relatively few studies have examined infusion of pre-synthesized nanocrystals into porous materials with carrier solvents. Such nanocrystals have been imbibed into the pores by capillary forces, in conjunction with additional driving forces including vacuum induction and electrophoresis.[16] With this technique, it can be challenging to fill the pores uniformly. Nanocrystals synthesized in the aqueous core of the reverse micelles have subsequently been infused into nanoporous matrixes.[17,18] The ability to isolate the particles from the unreacted precursors and to keep the particles coated with surfactant can be challenging in these micelles. Yet another approach is to entrap pre-synthesized nanocrystals during the synthesis of a nanoporous matrix, although the nanocrystals can in some cases perturb the geometry of the matrix.[7,19]

* Corresponding author. Fax: (512)471-7060. Telephone: (512)471-4617. E-mail: kpj@che.utexas.edu.

(1) Murray, C. B.; Norris, D. J.; Bawendi, M. G. *J. Am. Chem. Soc.* **1993**, *115*, 8706−8715.
(2) Brust, M.; Walker, M.; Bethell, D.; Schiffrin, D. J.; Whyman, R. *J. Chem. Soc., Chem. Commun.* **1994**, *7*, 801−802.
(3) Shah, P. S.; Husain, S.; Johnston, K. P.; Korgel, B. A. *J. Phys. Chem. B* **2001**, *105*, 9433−9440.
(4) Shah, P. S.; Husain, S.; Johnston, K. P.; Korgel, B. A. *J. Phys. Chem. B* **2002**, *106*, 12178−12185.
(5) Skaff, H.; Lin, Y.; Dinsmore, A.; Russell, T.; Emrick, T. *Abstracts of Papers, 224th ACS National Meeting*, Boston, MA, August 18−22, 2002; American Chemical Society: Washington, DC, 2002; COLL-026.
(6) Weimann, T.; Geyer, W.; Hinze, P.; Stadler, V.; Eck, W.; Golzhauser, A. *Microelectron. Eng.* **2001**, *57−58*, 903−907.
(7) Konya, Z.; Puntes, V. F.; Kiricsi, I.; Zhu, J.; Alivisatos, P.; Somorjai, G. A. *Catalysis Lett.* **2002**, *81*, 137−140.
(8) Wakayama, H.; Setoyama, N.; Fukushima, Y. *Adv. Mater.* **2003**, *15*, 742−745.
(9) Han, Y.-J.; Kim, J. M.; Stucky, G. D. *Chem. Mater.* **2000**, *12*, 2068−2069.
(10) Fukuoka, A.; Araki, H.; Sakamoto, Y.; Sugimoto, N.; Tsukada, H.; Kumai, Y.; Akimoto, Y.; Ichikawa, M. *Nano Lett.* **2002**, *2*, 793−795.
(11) Coleman, N. R. B.; Ryan, K. M.; Spalding, T. R.; Holmes, J. D.; Morris, M. A. *Chem. Phys. Lett.* **2001**, *343*, 1.
(12) Coleman, N. R. B.; O'Sullivan, N.; Ryan, K. M.; Crowley, T. A.; Morris, M. A.; Spalding, T. R.; Steytler, D. C.; Holmes, J. D. *J. Am. Chem. Soc.* **2001**, *123*, 7010.
(13) Chen, W.; Cai, W.; Zhang, L.; Wang, G.; Zhang, L. *J. Colloid Interface Sci.* **2001**, *238*, 291−295.
(14) Ryan, K. M.; Erts, D.; Olin, H.; Morris, M. S.; Holmes, J. D. *J. Am. Chem. Soc.* **2003**, *125*, 6284.
(15) Lake, L. W. *Enhanced Oil Recovery*; Prentice Hall, New York, 1996.
(16) Hornyak, G.; Kroll, M.; Pugin, R.; Sawitowski, T.; Schmid, G.; Bovin, J.-O.; Karsson, G.; Hofmeister, H.; Hopfe, S. *Chem.−Eur. J.* **1997**, *3*, 1951−1956.
(17) Hirai, T.; Okubo, H.; Komasawa, I. *J. Phys. Chem. B* **1999**, *103*, 4228−4230.
(18) Hirai, T.; Okubo, H.; Komasawa, I. *J. Colloid Interface Sci.* **2001**, *235*, 358−364.

10.1021/cm051052w CCC: $30.25
Published on Web 11/19/2005

Table 1. Methods for Loading of Metal Nanoparticles into Mesoporous Silica

nanoporous material	material impregnated	pore diameter (nm)	nanoparticle size (nm)	time, temp[a]	loading	method of loading	ref
FSM-16	Pt	2.4	2.3 (0.1	5 h, 423 K	0.9 wt %	reduction of infused precursor	8
FSM-16	Pt	3.5	2.9 (0.16	5 h, 423 K	2.9 wt %	reduction of infused precursor	8
thiol modified MCM41	CdS	3.8	3.3	12 h, 298 K		impregnation of nanocrystals from reverse micelle	18
planar-like monolithic	Au	5.7	5.2	3 weeks, 298 K		reduction of infused precursor by sonification	13
HMM-2	Au	$d_{100} = 2.2$	3.2 (0.5	24 h, 298 K	2 wt %	reduction of precursor	72
SBA-15	Pt	$d_{100} = 10.23$	2−5		10^{17} particles/gm silica	silica synthesis in presence of presynthesized nanocrystals	62
porous alumina membrane	Au	50	15			impregnation of nanocrystals by vacuum induction or by electrophoresis	16
hybrid inorganic−organic mesoporous silica	Au	3.6	3.4 (0.5	96 h, 298 K	3.1 wt %	reduction of Infused precursor	73
SBA-15	Au	8.8	2.2 (0.3	24 h, 308 K	2.3 wt %	impregnation of pre-synthesized nanocrystals	this work
MCM-41	Au	2.9	2.2 (0.3	24 h, 308 K	2.0 wt %	impregnation of pre-synthesized nanocrystals	this work
MCM-41	Au	2.4	2.2 (0.3	24 h, 308 K	1.7 wt %	impregnation of pre-synthesized nanocrystals	this work

[a] Time and temperature are only shown for the infusion of either the precursor or the pre-synthesized silica.

There are two primary challenges in the infusion of pre-synthesized nanocrystals into a nanoporous matrix. First, the nanocrystal dispersion must be transported through the pores by favorable capillary wetting, and the nanocrystals must not block small pore entrances. Once the nanocrystals penetrate the pores, the second challenge is to achieve sufficient adsorption of the nanocrystals from the solution phase to the substrate surface. A major dilemma must be addressed. The solvent must allow for enough attraction between the nanocrystals and substrate to achieve sufficient adsorption, while simultaneously preventing flocculation of nanocrystals in the solvent phase. The nanocrystals must be dispersed in "good" solvent for the stabilizing ligands to prevent flocculation. However, good solvents may be expected to cause the interactions between the nanocrystals and the surface of the nanoporous material to be repulsive or weakly attractive.[20] The resulting weak adsorption of the particles inside the pores may produce low loadings. Thus, the solvent must be tuned to provide a judicious balance between nanocrystal−nanocrystal versus nanocrystal−substrate interactions.

The penetration of reactive precursors into high aspect ratio features[21] and nanoporous materials such as activated carbon[22] is particularly efficient with supercritical fluids, due to high diffusion coefficients and low viscosities. Examples include the synthesis of porous silica fibers[23] and metal oxide fibers[24] within activated carbon fiber templates. Silicon and germanium nanowires have been synthesized in mesoporous silica from reactive precursors using sc-hexane and sc-CO_2, respectively.[25,26] High diffusivities in sc-CO_2 facilitate transport of the precursors into the pores. The miscibility between CO_2 and air or organic solvents often leads to favorable contact angles and wetting, as in the case of CO_2, enhanced oil recovery in small sandstone pores[27] and in the cleaning of low k nanoporous dielectric insulators.[28]

CO_2 is used extensively to swell organic solvents to lower the solvent strength to precipitate polymers from solution[29] and to form nanoparticles of many types of materials[30−33] including pharmaceuticals. The influence of CO_2 as an antisolvent on the solubility of solutes[34] and on spectral shifts of solvatochromic probes[35,36] has been determined over a wide range in CO_2 concentration. CO_2-expanded liquids (CXLs) have been exploited for homogeneous catalytic oxidations[37,38] and for hydrogenation and hydroformylation

(19) Konya, Z.; Puntes, V. F.; Kiricsi, I.; Zhu, J.; Ager, J. W., III; Ko, M. K.; Frei, H.; Alivisatos, P.; Somorjai, G. A. *Chem. Mater.* **2003**, *15*, 1242−1248.
(20) Israelachvili, J. *Intermolecular & Surface Forces*, 2nd ed.; Academic Press: San Diego, 1992.
(21) Watkins, J. J.; Blackburn, J. M.; McCarthy, T. J. *Chem. Mater.* **1999**, *11*, 213−215.
(22) Wakayama, H.; Fukushima, Y. *Ind. Eng. Chem. Res.* **2000**, *39*, 4641−4645.
(23) Fukushima, Y.; Wakayama, H. *J. Phys. Chem. B* **1999**, *103*, 3062−3064.
(24) Wakayama, H.; Itahara, H.; Tatsuda, N.; Inagaki, S.; Fukushima, Y. *Chem. Mater.* **2001**, *13*, 2392−2396.
(25) Coleman, N. R. B.; Morris, M. A.; Spalding, T. R.; Holmes, J. D. *J. Am. Chem. Soc.* **2001**, *123*, 187−188.
(26) Ziegler, K. J.; Polyakov, B.; Kulkarni, J. S.; Crowley, T. A.; Ryan, K. M.; Morris, M. A.; Erts, D.; Holmes, J. D. *J. Mater. Chem.* **2004**, *14*, 585−589.
(27) Van Bergen, F.; Gale, J.; Damen, K. J.; Wildenborg, A. F. B. *Energy (Amsterdam, Netherlands)* **2004**, *29*, 1611−1621.
(28) Zhang, X.; Pham, J. Q.; Martinez, H. J.; Wolf, P. J.; Green, P. F.; Johnston, K. P. *J. Vacuum Sci. Technol. B* **2003**, *21*, 2590−2598.
(29) McClellan, A. K.; McHugh, M. A. *Polym. Eng. Sci.* **1985**, *25*, 1088−1092.
(30) Gallagher, P. M.; Coffey, M. P.; Krukonis, V. J.; Klasuts, N. In *Supercritical Fluid Science and Technology*; Johnston, K. P., Ed.; American Chemical Society: Washington, DC, 1989; Vol. 406, pp 334−354.
(31) Dixon, D. J.; Bodmeier, R. A.; Johnston, K. P. *AIChE J.* **1993**, *39*, 127.
(32) Randolph, T. W.; Randolph, A. D.; Mebes, M.; Yeung, S. *Biotechnol. Prog.* **1993**, *9*, 429−435.
(33) Yeo, S.-D.; Debenedetti, P. G.; Radosz, M.; Schmidt, H.-W. *Macromolecules* **1993**, *26*, 6207−6210.
(34) Dixon, D. J.; Johnston, K. P. *AIChE J.* **1991**, *37*, 1441−1449.
(35) Maiwald, M.; Schneider, G. M. *Ber. Bunsen-Ges.* **1998**, *102*, 960−964.
(36) Kelley, S. P.; Lemert, R. M. *AIChE J.* **1996**, *42*, 2047−2056.
(37) Wei, M.; Musie, G. T.; Busch, D. H.; Subramanian, B. *J. Am. Chem. Soc.* **2002**, *124*, 2513−2517.

reactions.[39,40] The presence of CO_2 in the mixed medium increases the solubility of O_2 by 100 times and also improves diffusion rates. Tunable properties of CXLs has been utilized for the rapid and precise size selection of the nanocrystals.[41]

Herein, we show that the use of supercritical CO_2 as an antisolvent helps overcome both transport and thermodynamic challenges in nanoparticle infusion into porous materials. Our objective is to add CO_2 to an organic solvent (toluene) to achieve high levels of infusion of pre-synthesized nanocrystals into mesoporous silica within a 24 h period. The CO_2 concentration in toluene is tuned to produce sufficiently strong nanocrystal-silica interactions for high nanocrystal adsorption in the pores without flocculating the nanocrystals in the solvent phase. At 35 °C and pressures of this study above 68 bar,[42] CO_2 forms a homogeneous one-phase solution with toluene. Dodecanethiol-capped metal nanocrystals cannot be dispersed in pure CO_2;[4] however, they are soluble in our CO_2−toluene mixtures. The loading of the gold particles was determined by measuring spectrophotometrically the reduction in the absorbance of gold in the supernatant after separation from the mesoporous silica phase. As a control, the infusion was also studied (1) without CO_2 present and (2) with methanol as an antisolvent in toluene. The diameters of the porous cylinders in the mesoporous silica were varied from 2.5 to 9 nm. The kinetics of infusion was studied over a period of 3 to 72 h, both with and without CO_2, to understand the effect of changes in the transport properties of the nanocrystals. The effects of CO_2 on both the kinetics and the final loading are analyzed relative to nonexpanded liquid solvents, toluene or toluene−methanol mixtures. In the first part of the discussion section, we analyze the equilibrium loading and then examine the kinetic aspects in the second section.

A key advantage of impregnating pre-synthesized nanocrystals into pores is that the nanocrystal synthesis may be controlled with stabilizing ligands to produce the desired size, crystallinity, shape, and surface properties. Numerous synthetic schemes have been reported.[2] The nanocrystal morphology may be chosen independently of the pore morphology, as long as the crystals are smaller than the pores. Prior to infusion, the particles may be isolated from unwanted byproducts, cleaned, and separated by size, and the ligands may be exchanged if desired for alternative ligands. It would be difficult if not impossible to execute these post-reaction steps if the nanocrystals were synthesized inside the nanoporous material. Finally, synthesis inside nanoporous materials can be perturbed by surface chemistry due to the substrate; for example, capping ligands may adsorb to the substrate rather than the nanocrystals.

Experimental Section

All chemicals were used as received. Water used was doubly distilled and deionized. Hydrogen tetrachloroaurate(III) trihydrate ($HAuCl_4 \cdot 3H_2O$) (purity > 99.9%), tetraoctylammonium bromide ($(C_8H_{17})_4-NBr$) (purity > 98%), sodium borohydride ($NaBH_4$) (purity > 99%), and 1-dodecanethiol ($C_{12}H_{25}SH$) (purity > 98%) were purchased from Sigma-Aldrich Chemical Co. Toluene (99.9%) and concentrated liquid HCl (normality 12.1) were obtained from Fisher Scientific. Ethanol (Absolute 200 proof) was obtained from Aaper alcohol. Methanol (purity > 99.8%) was obtained from EM Sciences. Tetraethoxysilane (TEOS, $C_8H_{20}O_4Si$), hexadecyltrimethylammonium bromide ($C_{19}H_{42}NBr$) (purity > 96%), and decyltrimethylammonium bromide ($C_{13}H_{30}BrN$) (purity > 98%) were obtained from Fluka Chemika; poly(ethylene oxide)−poly(propylene oxide)−poly(ethylene oxide) $EO_{20}PO_{70}EO_{20}$ (Pluronic P-123) was from BASF Corporation. Carbon dioxide (purity > 99.99%) (Matheson Gas Products) was used as received. Polycarbonate filters (0.05 μm) were obtained from Osmonics.

Nanocrystal Synthesis. Gold nanocrystals were synthesized by a two-phase (organic−water) arrested precipitation technique,[2] using dodecanethiol ($C_{12}H_{25}SH$) as a capping agent. Initially, 36 mL of aqueous (0.03 M) hydrogen tetrachloroaurate(III) trihydrate ($HAuCl_4 \cdot 3H_2O$) was combined with 25 mL of toluene solution containing 2.7 gm of phase transfer catalyst, tetraoctylammonium bromide. After stirring for 1 h, the organic phase, with the transferred gold, was collected. The gold salt was then reduced using 15 mL of an aqueous sodium borohydride ($NaBH_4$) solution (0.44 M), resulting in gold nanocrystals dispersed in toluene, protected by the phase transfer catalyst. To this solution, 240 μL of dodecanethiol was added immediately and stirred overnight. The organic phase rich in gold nanocrystals was collected. Methanol was added to the organic phase, and the solution was centrifuged to separate the nanocrystals. The nanocrystals were washed and redispersed in 20 mL of toluene.

Mesoporous Silica Synthesis. Mesoporous silica SBA-15 was synthesized via a procedure similar to that reported by Zhao et al.[43] A solution of 1.6 g of $EO_{20}PO_{70}EO_{20}$:7 mL of HCl:8 mL of TEOS:38 mL of H_2O was prepared, stirred for 24 h at 50 °C, and then heated at 100 °C for 24 h. The resulting slightly yellow powder was dispersed in ethanol, filtered, and then again heated at 100 °C for 24 h. The yellow product was then calcined at 550 °C.

Mesoporous silica MCM-41 was synthesized by $S^+X^-I^+$ assembly via a procedure similar to that reported by Tanev and Pinnavaia.[44] $C_nH_{2n+1}N(CH_3)_3Br$ template ($n = 10, 16$) was used as a structure directing agent. Depending on the chain length of the surfactant, MCM-41 silica with different pore diameters was obtained. Small pore diameter silica (S-MCM41) was obtained with surfactant chain length $n = 10$, while large pore diameter silica (L-MCM41) was obtained with chain length $n = 16$.

For the synthesis of S-MCM41, a solution of 0.8 g of $C_{10}H_{21}N(CH_3)_3Br$:7 mL of HCl:5 mL of TEOS:38 mL of H_2O was prepared, stirred overnight at ambient temperature, and then heated at 100 °C for 6 h. The ratio of the components in the solution is different than that reported by Tanev and Pinnavaia.[44] The while powder was then dispersed in ethanol, filtered, and dried at 100 °C for 24 h. The collected solid was then calcined at 600 °C. The L-MCM41 was synthesized similarly to S-MCM41 except that a solution with a composition of 1.6 g of $C_{16}H_{33}N(CH_3)_3Br$:7 mL of HCl:8 mL of TEOS:38 mL of H_2O was used.

(38) Wei, M.; Musie, G. T.; Busch, D. H.; Subramanian, B. *Green Chem.* **2004**, *6*, 387−393.
(39) Xie, X.; Liotta, C. L.; Eckert, C. A. *Ind. Eng. Chem. Res.* **2004**, *43*, 7907−7911.
(40) Sellin, M. F.; Webb, P. B.; Cole-Hamilton, T. J. *Chem. Commun.* **2001**, 781−782.
(41) McLeod, M. C.; Anand, M.; Kitchens, C. L.; Roberts, C. B. *Nano Lett.* **2005**, *5*, 461−465.
(42) Ng, H.-J.; Robinson, D. B. *J. Chem. Eng. Data* **1978**, *23*, 325−327.
(43) Zhao, D.; Feng, J.; Huo, Q.; Melosh, N.; Frederickson, G. H.; Chmelka, B. F.; Stucky, G. D. *Science (Washington, D.C.)* **1998**, *279*, 548−552.
(44) Tanev, P. T.; Pinnavaia, T. J. *Chem. Mater.* **1996**, *8*, 2068−2079.

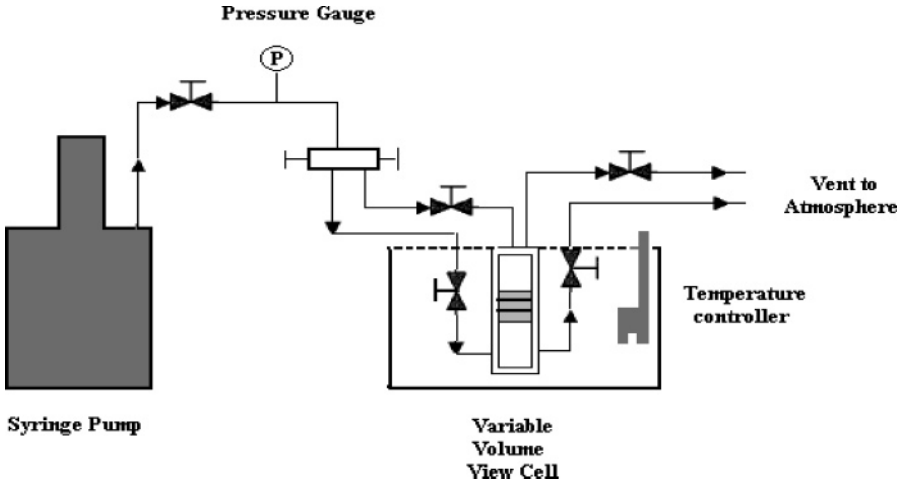

Figure 1. Schematic of reaction infusion apparatus.

Infusion Procedure. In a typical experiment, 20 mg of mesoporous silica and 2.5 mL of gold nanocrystals dispersed in toluene, with a concentration of 0.3 mg/mL, were loaded in the reaction cell with a working volume (volume with piston in the cell) of 27 mL. A total of 0−5 mL of toluene was added in the cell. The cell was then sealed, and an amount of CO_2 equivalent to 2.5−7.5 mL at 241 bar (3500 psi) and 35 °C was added so as to produce a total volume of reaction mixture of 10 mL. The cell was then pressurized to 241 bar with CO_2 at the backside of the piston using an ISCO model 100 DX computer-controlled syringe pump. The contents of the cell, in a water bath, were stirred using a magnetic stir bar that was inserted inside the cell (Figure 1). The reaction was maintained at 35 °C and 241 bar (3500 psi) and allowed to proceed for 24 h. After the reaction, the cell was cooled to 0 °C, and CO_2 was then vented as a vapor from the top of the cell, leaving most of the other components in the cell. Lowering the temperature to 0 °C reduces the loss of toluene vapor along with CO_2. The supernatant was collected and filtered, using a polycarbonate 0.05 μm filter, to separate the mesoporous silica. The volume of the supernatant was found to be slightly less than the total volume of gold feed solution and toluene added to the cell because of some toluene loss along with CO_2. The loss of toluene was usually about 5−6 vol %. The extent of incorporation of gold nanocrystals in the silica was determined by subtracting the final mass of the nanocrystals recovered in the supernatant from the initial mass of the nanocrystals. The absorbance of the gold nanocrystals dispersed in toluene before and after infusion was measured at a wavelength of 500 nm using a Cary 500 UV−Vis−NIR spectrophotometer to determine the nanocrystal mass. An optical path length of 1 cm was used. A standard calibration curve was generated at 500 nm using known concentrations of gold nanocrystals in toluene as shown in Figure 2. A typical starting gold concentration was 0.3 mg/mL, and after infusion the value decreased to 0.195 mg/mL for a loading of 2 wt % and to 0.17 mg/mL for a loading of 2.2 wt %. The experiments were repeated several times to check for the reproducibility, which was on the order of ± 0.3 in wt % units.

Characterization

The nanocrystal size and size distribution for the synthesized gold nanocrystals dispersed in toluene was determined using small-angle X-ray scattering (SAXS). SAXS was also used to determine the structure and the center-to-center distance between the pores of synthesized mesoporous silica. SAXS was performed using a rotating copper anode generator (Bruker Nonius) operated at 3.0 kW. Scattered photons

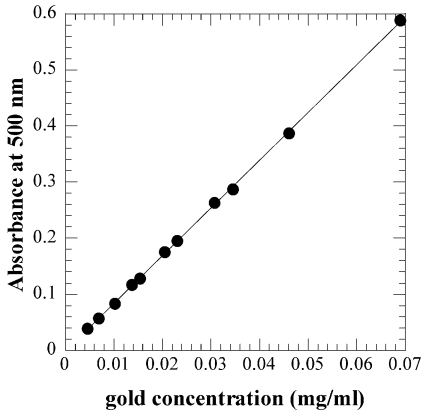

Figure 2. Calibration curve of UV−visible absorbance vs concentration of 2 nm gold nanocrystal dispersions in toluene, measured at wavelength of 500 nm.

were collected on a multiwire gas-filled detector (Molecular Metrology, Inc.). The scattering angle was calibrated using a silver behenate ($CH_3(CH_2)_{20}COOAg$) standard, and all experimental data were corrected for background scattering and sample absorption. Scattering data were collected from a dilute dispersion of gold nanocrystals in toluene and from dried powdered samples of silica.

N_2 porosimetry was used for obtaining the surface area and the pore size distribution of the mesoporous silica with a high-speed surface area BET analyzer (NOVA 2000, Quantachrome Instruments, Boynton Beach, FL) at a temperature of 77 K. Silica samples were pretreated at 100 °C for 24 h in a vacuum immediately prior to data collection. Pore size distributions were analyzed by using the adsorption branch of the isotherm. The Barrett- Joyner- Halenda (BJH) method[45] was used for SBA-15, while the Saito−Foley (SF) method was used for S-MCM41 and L-MCM41.[46] The SF method is similar to the HK method[47] but takes into consideration the cylindrical geometry of the pores.

Low-resolution pictures of mesoporous silica, infused with gold nanocrystals, were visualized by TEM on a Phillips EM280 microscope with a 4.5 Å point-to-point resolution

(45) Barrett, E. P.; Joyner, L. G.; Halenda, P. P. *J. Am. Chem. Soc.* **1951**, *73*, 373−380.
(46) Saito, A.; Foley, H. C. *AIChE J.* **1991**, *37*, 429−436.
(47) Horvath, G.; Kawazoe, K. *J. Chem. Eng. Jpn.* **1983**, *16*, 470−475.

operated with an 80 kV accelerating voltage. High-resolution transmission electron microscopy (HRTEM) was performed using a JEOL 2010F TEM operating at 200 kV. Images were obtained primarily with a GATAN digital photography system. Silica particles were deposited from a dilute chloroform solution onto 200 mesh carbon-coated copper TEM grids (Electron Microscopy Sciences).

Results

Nanoparticle Characterization. SAXS was used to characterize mesoporous silica structure as well as the gold nanocrystal dispersions. The intensity of scattered radiation, $I(q)$, is proportional to a shape factor and structure factor, $P(q)$ and $S(q)$, respectively: $I(q) \propto P(q)S(q)$. Here, q is the wave vector, defined as $q = 4\pi/\lambda \sin(\theta)$, where λ is the wavelength (0.154 nm) and 2θ is the scattering angle. The wave vector is also inversely proportional to a characteristic distance (d) in the scattering system: $q = 2\pi/d$. The shape factor is related to the size and shape of the scatterers, whereas the structure factor contains information about interactions or ordering within the system.

For dilute solutions of non-interacting nanocrystals $S(q) = 1$, and the scattered intensity relates only the shape factor of the particles dispersed in solution (i.e., $I(q) \propto P(q)$).[48−51] The shape factor for spherical particles is given analytically by[52,53] $P(q) = [3(\sin(qR) - qR\cos(qR))/(qR)^3]^2$, where R is the nanocrystal radius. The effects of sample polydispersity on the scattered intensity can be taken into account using $I(q) \propto \int N(R)P(q)R^6\, dR$, where $N(R)$ is a normalized size distribution.[48,54] Here the size distribution is assumed to be Gaussian, where R_{avg} and σ are the average radius and standard deviation, respectively. Fitting this model to the scattering data from the toluene dispersion of gold nanocrystals (Figure 3) indicates that the gold nanocrystals were relatively monodisperse with a mean diameter of 2.2 ± 0.3 nm. The curve in Figure 3 does not show any peaks, indicating weak interactions between the particles due to the good solvation of the ligands, as seen previously for nanocrystals in pure organic solvents.[54] In contrast, strong attractive interactions of perfluoropolyether coated gold nanoparticles have been observed with SAXS in CO_2 due to the stronger Hamaker interactions between the cores, and the limited solvation of the ligands, both resulting from the weak solvent strength.[55]

Characterization of Mesoporous Silica. SAXS was used to characterize the mesoporous silica powders prior to infusion. Highly oriented pores, arranged in a 2-D hexagonal lattice, give rise to a series of Bragg peaks in the scattering pattern. Figure 4 and Table 2 give the small angle XRD pattern for three mesoporous silicas: SBA-15 (a), L-MCM41 (b), and S-MCM41 (c). For SBA-15, the four well-resolved peaks are indexable as the (100), (110), (200), and (210) reflections associated with p6 mm hexagonal symmetry. One additional weak peak is found at q (nm^{-1}) = 1.82 and corresponds to a (300) reflection. Presence of multiple sharp peaks indicates that calcined SBA-15 has a high degree of hexagonal mesoscopic organization. The first three peaks for SBA-15 are located at $q_{100} = 0.61$, $q_{110} = 1.06$, and $q_{200} = 1.22$ nm^{-1} with the peak position ratio of $1:\sqrt{3}:2$, which is consistent with the literature.[56−58] The distance d_{100} between adjacent planes is given by $d_{100} = 2\pi/q_{100} = 10.29$ nm. The unit cell parameter $a_0 = 2d_{100}/\sqrt{3} = 11.9$ nm gives the center-to-center spacings of the pores and agrees fairly with the literature.[43]

L-MCM41 shows two indexable peaks corresponding to (100) and (110) reflections. The peaks are broad and show diffuse scattering centered at $q = 1.63$ nm^{-1} corresponding to reflection from the (100) plane, which manifests a lower

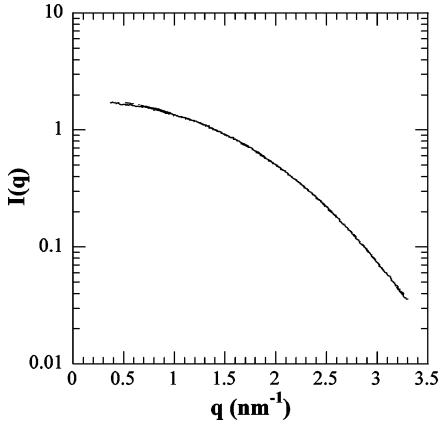

Figure 3. Intensity $I(q)$ vs wave vector (q) for gold nanocrystals dispersed in toluene determined by SAXS.

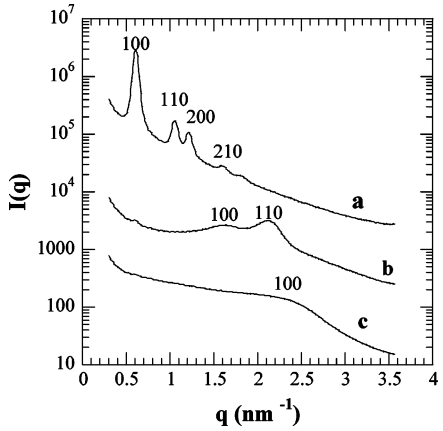

Figure 4. SAXS for calcined mesoporous silica SBA-15 (a), L-MCM41 (b), and S-MCM41 (c).

(48) Lifshin, E. *X-ray Characterization of Materials*; Wiley-VCH: New York, 1999.
(49) Korgel, B. A.; Fitzmaurice, D. *Phys. Rev. B* **1999**, *59*, 14191−14201.
(50) Mattoussi, H.; Cumming, A. W.; Murray, C. B.; Bawendi, M. G.; Ober, R. *Phys. Rev. B* **1998**, *58*, 7850−7863.
(51) Korgel, B. A.; Fullam, S.; Connolly, S.; Fitzmaurice, D. *J. Phys. Chem. B* **1998**, *102*, 8379−8388.
(52) Guinier, A.; Fournet, G. *Small-Angle Scattering of X-rays*; Wiley: New York, 1955.
(53) Glatter, O.; Kratky, O. *Small-Angle X-ray Scattering*; Academic Press Inc: New York, 1982.
(54) Saunders, A. E.; Korgel, B. A. *J. Phys. Chem. B* **2004**, *108*, 16732−16738.
(55) Saunders, A. E.; Shah, P. S.; Park, E. J.; Lim, K. T.; Johnston, K. P.; Korgel, B. A. *J. Phys. Chem.* B **2004**, *108*, 15969−15975.
(56) Lee, J.; Park, Y.; Kim, P.; Kim, H.; Yi, J. *J. Mater. Chem.* **2004**, *14*, 1050−1056.
(57) Ehrburger-Dolle, F.; Morfin, I.; Geissler, E.; Bley, F.; Livet, F.; Vix-Guterl, C.; Saadallah, S.; Parmentier, J.; Reda, M.; Patarin, J.; Iliescu, M.; Werckmann, J. *Langmuir* **2003**, *19*, 4303−4308.
(58) Kresge, C. T.; Leonowickz, M. E.; Roth, W. J.; Beck, J. S. *Nature* **1992**, *359*, 710.

Table 2. Properties of Mesoporous Silica

silica	center−center distance between pores, a_o (nm)	pore diameter	wall thickness (nm)	surface area (m^2/g)	pore volume (mL/gm)	no. of pores/ g of silica $\times 10^{-15}$[a]	surfactant
SBA-15	11.9	8.8	3.1	700	1.09	2.5	$EO_{20}PO_{70}EO_{20}$
L-MCM41	4.4	2.9	1.5	825	0.55	8.8	$C_{19}H_{42}NBr$
S-MCM41	3.4	2.4	1.0	738	0.38	9.8	$C_{13}H_{30}NBr$

[a] Based on surface area. Average length of the pore was considered 10 μm for all three mesoporous silica.

degree of order as compared to SBA-15. The distance d_{100} between adjacent planes is 3.85 nm, and the unit cell parameter $a_0 = 4.44$ nm for L-MCM41. S-MCM41 exhibits single d_{100} reflections accompanied by a diffuse scattering centered at $\sim$ 2.95 nm with a unit cell parameter of 3.4 nm. Pinnavaia et al. have demonstrated that "single-reflection" MCM-41 still can have short ranged hexagonal symmetry.[44,59] They show that MCM-41 synthesized by acidic $S^+X^-I^+$ pathway with surfactant chain length < 14 result in poorly ordered products. For S-MCM41, the lower degree of order can be attributed to the small chain length of only 10 for the structure directing agent.

Figure 5 gives the adsorption−desorption isotherms for the three calcined silica samples. Representative nitrogen adsorption−desorption isotherms and corresponding pore size distribution (BJH method) are shown in Figure 5a. SBA-15 had a mean pore diameter of 8.8 nm, BET surface area of 700 m^2/g, and a pore volume of 1.09 cm^3/gm (refer to Table 2), consistent with the literature.[43] Three well-distinguished regions of the adsorption isotherm are evident: (i) monolayer−multilayer adsorption, (ii) capillary condensation, and (iii) multilayer adsorption on the outer particle surfaces. The approximate pore size calculated using the BJH analysis is significantly smaller than the center-to-center distance between adjacent pores determined by SAXS, because the later includes the thickness of the pore wall. From the difference in these two values, the thickness of the pore wall is estimated to be 3.1 nm for SBA-15, which is in excellent agreement with the values reported by Zhao et al.[43] The adsorption−desorption isotherm for L-MCM41 and S-MCM41 and their corresponding pore size distributions, determined by SF method,[46] are shown in Figure 5, panels b and c, respectively, and Table 2.

As can be seen in Figure 5a, SBA-15 shows a type-H1 hysteresis loop with capillary condensation at a relative pressure of $P/P_0 = 0.7$.[43] The step in the hysteresis loop is very steep with a jump from 300 to 700 cm^3/g due to capillary condensation. The slope and the height of the step are clear indications of very well-defined mesopores with narrow pore size distribtution,[44] which is further substantiated by the multiple peaks arising in SAXS (Figure 4).

MCM-41 (Figure 5, panels b and c) shows a type 4 adsorption isotherm[44] with a small degree of hysteresis. This behavior is typical of MCM-41.[44] The pore sizes of 2.5 and 2.9 nm are smaller as compared to that of SBA-15. The adsorption increases gradually with an increase of P/P_0 without a steep jump, which suggests that the pores have a wider pore size distribution than for SBA-15. The surface areas obtained for L-MCM41 and S-MCM41 were 825 and 738 m^2/g, respectively, and are typical for MCM-41 mesoporous silica. The adsorption volume, for P/P_0 approaching unity, becomes the pore volume due to complete condensation of N_2. The pore volume increases from S-MCM41 to SBA-15 (refer to Table 2) resulting in increase of the adsorption volumes at STP.

Nanoparticle Dispersibility in Toluene−CO_2 Solution. To date only fluorinated ligands have been shown to disperse nanocrystals in pure CO_2.[3,4,60,61] However, we show that standard alkane capped nanocrystals may be dispersed in the toluene−CO_2 cosolvent system. Nanocrystal dispersions were analyzed with a Cary 3E UV−vis spectrophotometer in a vertically mounted variable-volume high-pressure optical cell with a path length of 2 cm. The temperature was controlled at 35 °C with heating tape and the pressure was 241 bar. At a 50 vol % concentration of CO_2 in the solution, the absorbance at 500 nm remained at 1.92 ± 0.02 for a period of 8 h indicating a stable dispersion.

Effect of CO_2 Concentration on Loading of Gold Nanocrystals in Mesoporous Silica. Figure 6 shows the loadings of the nanocrystals in mesoporous silica as a function of CO_2 concentration. For nanocrystals dispersed in pure toluene, there is virtually no infusion into the pores, as loadings were less than 0.1 wt %. The loadings increase linearly with CO_2 concentrations of 25% and 50% and then level off at the highest value of 75%. It is not possible to go to higher CO_2 concentrations, as the particles become unstable and start to precipitate, indicating insufficient solvation of the hydrocarbon capping ligands.

To investigate the effect of hydrostatic pressure on trapped air in the pores, infusion was conducted in pure toluene at 241 bar, in absence of carbon dioxide. Air may potentially be trapped between two liquid domains at both ends of a cylindrical pore. A very small loading of 0.3 wt % was observed indicating that trapped air had little effect. The pores in the silica are interconnected to each other via small diameter channels. Perhaps the high-pressure forced some of the particles into these interconnects between pores.[15]

For CO_2−toluene mixtures, the relatively large loadings above 2% comparable to those obtained by the other infusion techniques in Table 1. We estimate, based on the molecular weight of the nanocrystals (50 000 g/mol of nanocrystals), a loading of about $10^{17}-10^{18}$ nanocrystals/g of silica, for each of our types of silica. A rough estimate of the order of number of pores per gm of silica (N) can be made from the specific surface area. For a surface area (S) of 1000 m^2/g

(59) Tanev, P. T.; Pinnavaia, T. J. *Science (Washington, D. C.)* **1995**, *267*, 865−867.

(60) Shah, P. S.; Holmes, J. D.; Doty, R. C.; Johnston, K. P.; Korgel, B. A. *J. Am. Chem. Soc.* **2000**, *122*, 4245−4246.

(61) Shah, P. S.; Novick, B. J.; Hwang, H. S.; Lim, K. T.; Carbonell, R. G.; Johnston, K. P.; Korgel, B. A. *Nano Lett.* **2003**, *3*, 1671−1675.

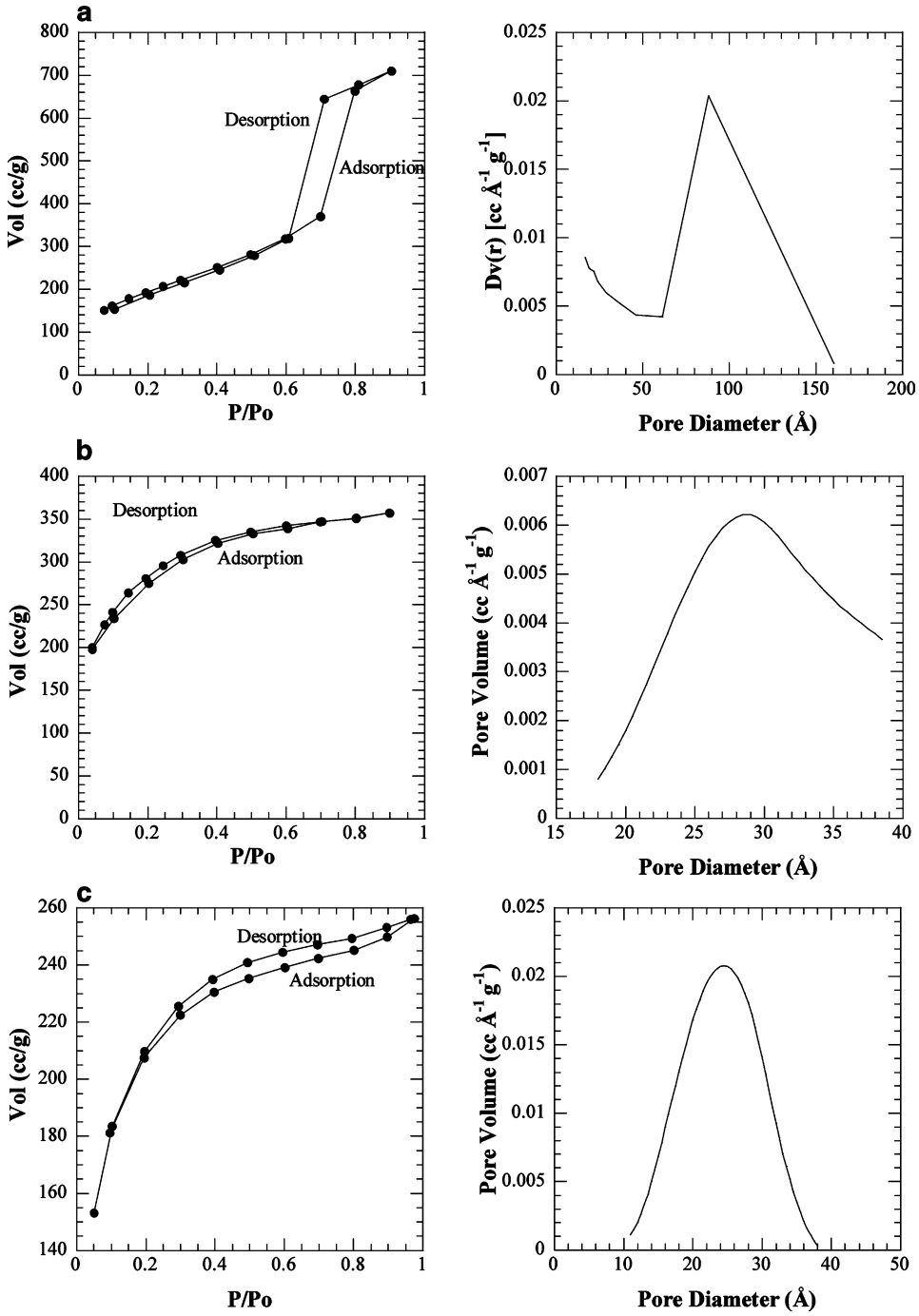

Figure 5. N_2 adsorption−desorption isotherms and corresponding pore size distributions for SBA-15 (a), L-MCM41 (b), and S-MCM41 (c).

and a radius (r) of 1 nm and pore length (l) of 10 μm (assuming that the pore length is equal to the particle size), we estimate from $N = S/(2\pi rl)$ that there are about 10^{16}−10^{17} pores per gram of silica. According to this estimate, our loading was about 10−100 particles per pore on average, consistent with the large number of particles in the TEMs in Figure 9. Konya et al.[62] obtained 10^{16} particles per gram of mesoporous silica, roughly equal to 2 particles per pore, which corresponds to 10^{16} pores per gram, similar to our value. It is important to note that we have obtained about 10 times higher loadings than Konya et al.[62] In our experiments, even at loadings of 2%, the crystal structure of the silica is intact as can be seen from TEM (Figure 9). At higher loadings Konya et al.[62] observed that the crystallinity of the silica decreased and worm like channels appeared due to the presence of the nanocrystals.

Effect of Pore Size and Concentration of Nanocrystals on the Loading of Nanocrystals. Figure 7 shows that the loadings of nanocrystals in the S-MCM41, L-MCM41, and SBA-15 silica from pure toluene dispersions were negligible. However, with the addition of 50% CO_2 the loadings were large in all cases and increased modestly with the pore diameter from 1.7% to 2.4%. The loading of the 2.2 nm particles into the silica with 2.4 nm pores was well over half

(62) Konya, Z. P.; Victor F.; Kiricsi, Imre; Zhu, Ji; Alivisatos, A. Paul; Somorjai, Gabor, A. *Nano Lett.* **2002**, *2*, 907−910.

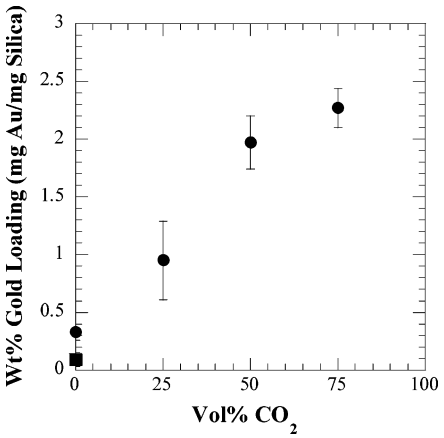

Figure 6. Loading of 2 nm gold nanocrystals dispersed in toluene−CO_2 cosolvent vs vol % concentration of CO_2 in cosolvent for 24 h impregnation period in L-MCM41. (■) 1 bar and 23 °C; (●) 241 bar and 35 °C.

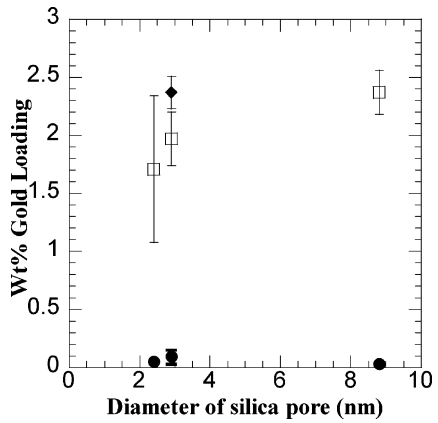

Figure 7. Loading of gold nanocrystals vs the pore diameter of silica. (□) loadings at 50 vol % CO_2, (●) loading at 0 vol % CO_2, and (◆) loading at 50 vol % CO_2 with the initial feed at 10 times higher concentration.

the loading for silica with 8.8 nm pores. Thus the diameters of the pores along the pore length appeared to be relatively uniform such that the particles did not block many narrow regions. The surface areas were similar for the three types of silica. The concentration of gold in the feed solution was increased 10-fold for L-MCM41 to 3 mg/mL, as shown in Figure 7. The loading increased a moderate amount from 2.0% to 2.4%.

Kinetic Study of the Infusion Process. For pure toluene, the nanocrystal loadings were negligible even after 7 days. Detailed kinetic studies were performed for 50% CO_2 with the silica with the smallest pores, S-MCM41. Here the mean diameter of the gold nanocrystals was 1.95 nm with a standard deviation/mean of 14% in contrast with the somewhat larger nanocrystals for our other systems. The loadings increased with time but appeared to reach an asymptote at 72 h, suggesting an approach to equilibrium (Figure 8). Over the first 24 h, where most of the infusion occurred, the loading was linear in $t^{1/2}$ as shown in Figure 8a.

TEM Micrographs of Infused Silica. Figure 9 shows typical images of gold nanocrystals infused in the three types of silica. The pore sizes and structures appear to be uniform. In each case, large numbers of highly dispersed nanocrystals are present in each pore, consistent with the estimate of about 100 particles/pore above. The presence of large numbers of nanocrystals throughout each pore corroborates the relatively

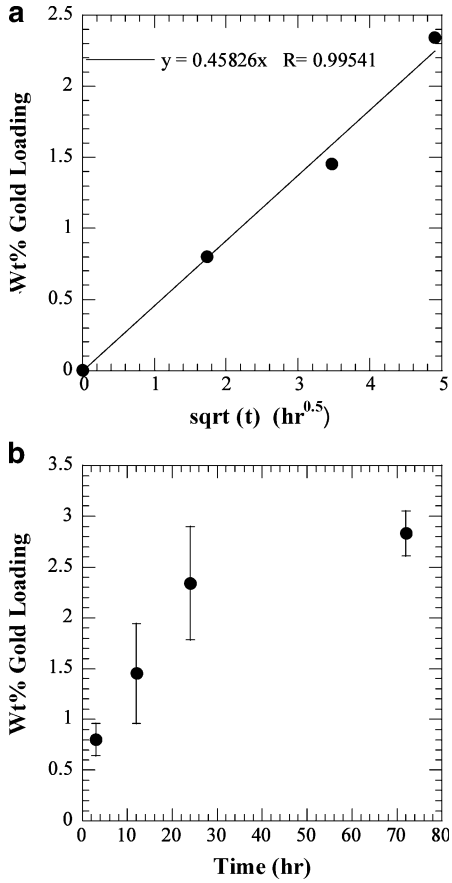

Figure 8. Gold nanocrystal loading vs time of impregnation for S-MCM41. (a) Loading vs $t^{1/2}$ for up to 24 h with a correlation coefficient of 99.5%. (b) Loading vs time with an approach to equilibrium.

high loadings measured by spectroscopy in Table 1. The presence of large number of particles in the pores was most likely for SBA-15 where the pore diameter is more than 4 times the diameter of the nanocrystals. Hence, the adsorption of a nanocrystal in the pore would be less likely to block the entry of a second nanocrystal. However, in the case of L-MCM41 and S-MCM41, where the ratio of the diameter of pore to the diameter of the particle is less than 2, the chances of pore blocking were much larger. Thus, the presence of large numbers of particles in each pore suggests that the adsorbed particles are mobile and can move toward the center of the pore by diffusion on the surface and/or in the bulk.

Effect of a Conventional Liquid Anti-solvent on Infusion. The effect of a liquid antisolvent, methanol, on the loading was used as a control experiment to shed further insight into the above experiments for the supercritical antisolvent, CO_2. Polar solvents are utilized as antisolvents for size selective precipitation of alkanethiol coated nanocrystals.[2] The addition of methanol may influence the nanocrystal−solvent−silica interactions but will not lower the viscosity of the solvent as is the case for CO_2. It was observed visually that gold nanocrystals at a concentration of 0.3 mg/mL dispersed in 50% methanol concentrations were stable for at least 24 h. At a level of 55% methanol−45% toluene, the dispersions became unstable with a visible settling front in less than 1 h. To adsorb nanocrystals in the pores without aggregation in the solvent mixture, we chose

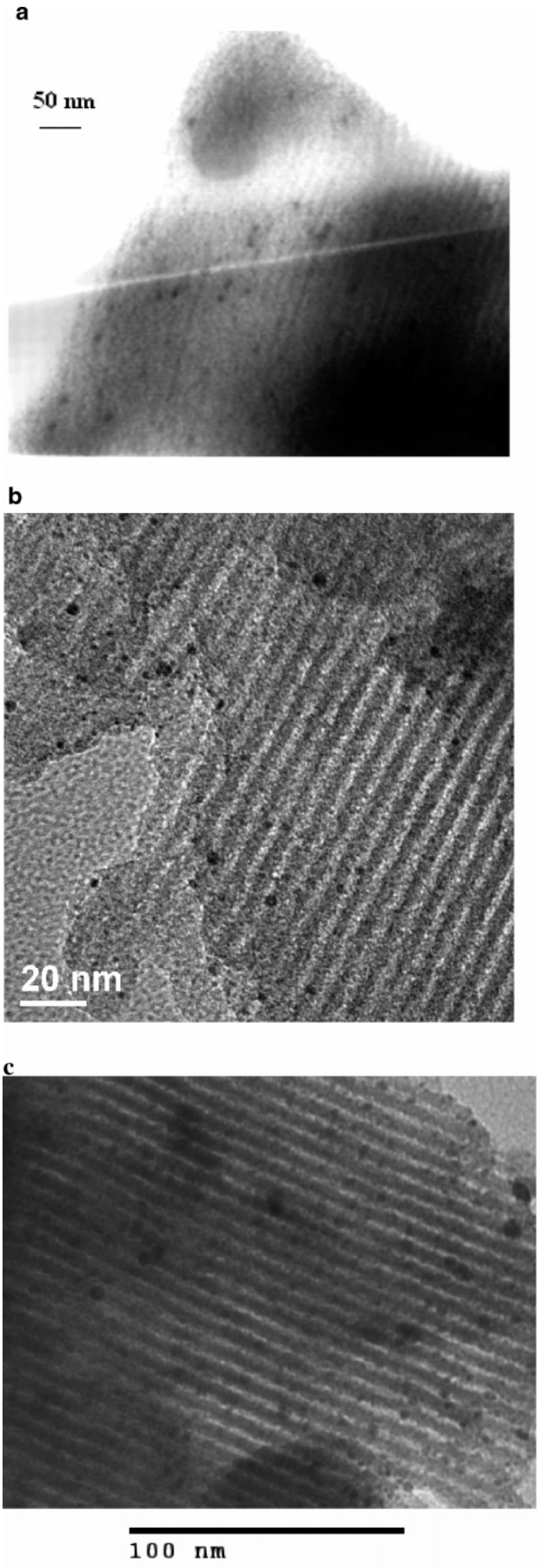

Figure 9. Representative TEM images of gold impregnated SBA-15 (a), L-MCM41 (b), and S-MCM41 (c).

a methanol concentration of 50% for the infusion experiments.

An amount of 20 mg of S-MCM41 was added to a 10 mL stirred solution of 1.95 nm gold nanocrystals (0.4 mg/mL). After 24 h, the loading was 0.56 ± 0.50%. After 7 days it reached 0.80 ± 0.18%, suggesting that the differences for methanol and CO_2 are not due simply to kinetic factors. These two loadings are within the experimental uncertainty indicating that the system approached equilibrium within 24 h. These loadings are less than half of the values obtained with CO_2.

Discussion

We begin by demonstrating that toluene wets the pores rapidly, and thus capillary wetting does not limit the infusion of the nanocrystals. The capillary forces become substantial for the cylindrical nanopores as described by the Laplace pressure

$$\Delta P = \frac{2\gamma_{LV}\cos\theta}{R} \tag{1}$$

where γ_{LV} is the surface tension of the liquid, R is the pore radius, and θ is the contact angle between the surface of the pore and the liquid. Toluene, with a surface tension of 28 dyn/cm wets silica with a contact angle of about 6°.[20] The Laplace pressure for wetting of a 4 nm pore for a toluene−silica−air interface of 278 bar provides a strong driving force for capillary wetting. On the basis of the conservative assumption that the initial air in the pores does not dissolve in toluene (if toluene is already presaturated with air), the air will be compressed from 1 to 278 bar and occupy a negligible volume, even if it is not displaced through one of the pore ends. Thus almost all of the pore volume will be available to the toluene. The capillary wetting by each of the other solvent mixtures in this study will also be favorable, as the contact angles will be well below 90°.

The rate at which the liquid solvent penetrates the pores can be estimated using the Washburn equation (combination of Laplace and Poiseuille equations):[63]

$$\frac{dh}{dt} = \frac{\gamma R\cos\theta}{4\eta h} \tag{2}$$

where η is the bulk viscosity. For cylindrical pores that extend the length of the particle, h is on the order of 20 μm. The time to fill a 4 nm diameter pore, determined from the integrated form of eq 8, is on the order of the order of 10^{-4} s. Thus, the diffusion and adsorption of the nanocrystals in the pores required several orders of magnitude more time than solvent infusion.

Equilibrium Nanocrystal Loading. In each of the solvents, pure toluene, toluene−CO_2, and toluene−methanol, the nanocrystal loading did not increase significantly after 24 h, indicating an approach to equilibrium. For toluene−CO_2, the similar loadings for the three types of mesoporous silica are consistent with the similar surface areas, despite

(63) Hiemenz, P. C. *Principles of Colloid and Surface Chemistry*; Marcel Dekker: New York, 1986.

the difference in pore diameters. The difference in pore diameter did not appear to cause an appreciable difference in the loading kinetics. The similar loadings for the similar surface areas suggest that the loadings approached equilibrium. The equilibrium adsorption of a nanocrystal in a pore onto the silica surface may be expected to be driven primarily by the chemical potential of the nanocrystals in the solvent and long-ranged van der Waals forces between the particles and silica surface, since the ligands are nonpolar. For simplicity, we treat the silica surface as a flat wall. The Hamaker constant A_{132}, for a gold particle (1) and silica surface (2) across a medium (toluene−CO_2 mixture, 3) may be approximated by[20]

$$A_{132} = (\sqrt{A_{11}} - \sqrt{A_{33}})(\sqrt{A_{22}} - \sqrt{A_{33}}) \quad (3)$$

where A_{ii} is the Hamaker constant for pure i, which can be estimated using a simplification of the Lifshift theory:[20]

$$A_{yy} = \frac{3}{4}k_b T\left(\frac{\epsilon_y - \epsilon_{vacuum}}{\epsilon_y + \epsilon_{vacuum}}\right)^2 + \frac{3h\nu_e}{16\sqrt{2}}\frac{(n_y^2 - n_{vacuum}^2)^2}{(n_y^2 + n_{vacuum}^2)^{3/2}} \quad (4)$$

where ν_e is the maximum electronic ultraviolet adsorption frequency, typically assumed to be 3×10^{15} s^{-1}.[4] The A for gold (4×10^{-19} J[20]), the ϵ and n for silica (3.91 and 1.45, respectively[64,65]), and for toluene (2.38 and 1.496, respectively[66,67]) were taken from the literature. The Hamaker constants for silica and toluene calculated from eq 2 are 5.97×10^{-20} J and 6.98×10^{-20} J, respectively.

The A_{33} was determined for the binary solvent mixture from eq 4 along with the Lorenz−Lorenz mixing rule:

$$(n_{mix} - 1)^2/(n_{mix} + 2)^2 = \sum \phi_i (n_i - 1)^2/(n_i + 2)^2 \quad (5)$$

where ϕ_i is the volume fraction of component i. An equivalent expression for the dielectric constant is obtained by replacing n with $\epsilon^{1/2}$ in eq 5. The n and ϵ for CO_2 were obtained as a function of density from the following:[68]

$$\frac{n^2 - 1}{n^2 + 2} = 0.07016\rho_r + 1.412 \times 10^{-4}\rho_r^2 - 3.171 \times 10^{-4}\rho_r^3 \quad (6)$$

$$\epsilon - 1 = 0.2386\rho_r + 0.02602\rho_r^2 \quad (7)$$

where $\rho_r = \rho/\rho_c$. At the reaction conditions of 241 bar and 35 °C, the n and ϵ for CO_2 were determined to be 1.2 and 1.12, respectively. The A for the pure CO_2 was calculated from eq 2 to be 1.44×10^{-20} J. The results for A_{33} are summarized in Table 3.

The Hamaker constant for the gold−silica interaction across pure toluene, A_{132}, turns out to be negative, indicating an unfavorable driving force for adsorption of the nanocrystals. The very low loading of nanocrystals from pure toluene is consistent with this result. With the addition of CO_2, A_{132} becomes increasingly positive, which would lead to an increase in the adsorption as observed. The loadings are correlated with the particle−silica van der Waals forces as characterized by A_{132} as listed in Table 3, which becomes more attractive with an increase in CO_2 concentration. In addition, the solvation of the nanocrystals in the solvent phase decreases with added CO_2 increasing the chemical potential of the nanocrystals. Both of these factors will produce stronger adsorption resulting in higher loadings, as observed.

Table 3. Overall Hamaker Constants A_{132} between Silica Surface and Gold Core Mediated by Supercritical CO_2−Toluene Solution[a]

vol % CO_2	$A_{33} \times 10^{20}$ (J)[b]	$A_{132} \times 10^{20}$ (J)
100	1.44	6.38
75	2.81	3.57
50	4.19	1.70
25	5.56	0.34
0	6.93	−0.31

[a] Component 1 is gold, 2 is SiO_2, and 3 is a mixture of toluene and CO_2. [b] Hamaker constant of solvent interacting with itself in vacuum.

Table 4. Overall Hamaker Constants A_{132} between Silica Surface and Gold Core Mediated by Methanol−Toluene Solution[a]

vol % methanol	$A_{33} \times 10^{20}$ (J)[b]	$A_{132} \times 10^{20}$ (J)
50	5.84	0.52
40	6.05	0.34
30	6.27	0.17
20	6.49	0.003
10	6.71	−0.16
0	6.93	−0.23

[a] Component 1 is gold, 2 is SiO_2, and 3 is a mixture of toluene and methanol. [b] Hamaker constant of solvent interacting with itself in vacuum.

This type of analysis was also applied to methanol as an antisolvent (Table 4). For 20% methanol, A_{132} becomes positive, indicating attractive van der Waals forces. The A_{132} value with 50% methanol is much weaker than in the case of only 25% CO_2. Therefore, the much weaker adsorption for methanol as an antisolvent relative to CO_2 is consistent with the A_{132} values.

Pure CO_2, with an exceptionally low polarizability/volume[60] has a much lower A than methanol or just about any other antisolvent. For example, CO_2 produces a greater reduction in A when added to toluene than does methanol. As the A of the intervening solvent, A_{33}, decreases, A_{132} always becomes less negative or more positive in eq 1, thus favoring adsorption. Therefore, CO_2 provides an opportunity to achieve a greater range in the tunability of a mixed solvent, which in our case plays a key role in achieving high nanocrystal loadings.

Transport Aspects of Nanocrystal Loading. Koone and Zerda[69] reported that the diffusion coefficient of water in a nanoporous glass of diameter 2.9 nm is of the order of 4×10^{-10} m^2/s, while the diffusion coefficient of water in the unbound system was 2.2×10^{-9} m^2/s. A much greater reduction in diffusion rate may be expected for the nanocrystals in the pores due to the much higher aspect ratio or solute size to pore diameter. Vigne-Maeder et al. performed molecular dynamics simulations of the diffusion of gases in

(64) Hourri, A.; St-Arnaud, J. M.; Bose, T. K. *J. Chem. Phys.* **1997**, *106*, 1780−1785.
(65) Burns, R. C.; Graham, C.; Weller, A. R. M. *Mol. Phys.* **1986**, *59*, 41.
(66) Rubio, J. E. F.; Arsuaga, J. M.; Taravillo, M.; Baonza, V. G.; Caceres, M. *Exp. Thermal Fluid Sci.* **2004**, *28*, 887−891.
(67) Williams, J. W.; Krchma, I. J. *J. Am. Chem. Soc.* **1926**, *48*, 1888−1896.
(68) Lewis, J. E.; Biswas, R.; Robinson, A. G.; Maroncelli, M. *J. Phys. Chem. B* **2001**, *105*, 3306−3318.
(69) Koone, N. D.; Zerda, T. W. *J. Non-Cryst. Solids* **1995**, *183*, 243−251.

zeolites.[70] The primary mechanism for transport was adsorption followed by surface diffusion to a pore mouth, rather than direct entrance to the pore. The importance of surface diffusion increased as the aspect ratio of particle diameter to pore diameter increased.

The nanocrystals diffuse from the entrance of the pore at both ends toward the center along the concentration gradient. The diffusion will take place both in the solvent within the pore and on the surface. In Figure 8a, the loading of the nanocrystals is plotted as a function of $t^{1/2}$ with a correlation coefficient of 0.995. According to the Stokes−Einstein relationship the diffusion coefficient of 2 nm gold nanocrystals in bulk toluene is 2×10^{-10} m^2/s. However, the actual diffusion coefficient in the pores was lower due to confinement in that it took about 24 h to approach the equilibrium loading as seen in Figure 8b. The effective diffusion coefficient in the pores of length l, including surface diffusion,[71] may be approximated by the equation $l = \sqrt{Dt}$. For 10 μm long pores in the particles, the diffusion coefficient was calculated to be 10^{-15} m^2/s.

When the diameter of the pore approaches that of the particle, the mass transfer resistance for the entry of the particle into the pore increases significantly and diffusion through the pore becomes considerably difficult. The aspect ratios, or particle/pore diameters are 0.9, 0.76, and 0.25 for the three silica. The slight increase in the loadings with the pore diameter (Figure 7) can be attributed to the larger pores and the increase in the structural ordering. The degree of order was shown to increase with an increase in pore size. The presence of well-ordered uniform cylindrical pores would lead to less pore blockage than disordered pores. As seen from the SAXS data, the degree of long-range ordering is highest for SBA-15 followed by L-MCM41, and finally S-MCM41 with limited order. It is observed that the even with relatively small order in S-MCM41, the loadings are significant, indicating that kinetic limitations were minor.

The similar loadings for the three silica with similar surface areas suggests that blocking of pores by nanocrystals is not significant. In the case of S-MCM41 where the aspect ratio of the particle to the pore is 0.9, surface diffusion must have been significant to prevent blocking of the pores. For this high aspect ratio, the polydispersity was rather low, otherwise, many smaller pores would not have been accessible.

Conclusions

A novel approach is presented to infuse pre-synthesized gold nanocrystals into preformed mesoporous silica by tuning the solvent quality with CO_2 as an antisolvent. The concept of decoupling the nanocrystal synthesis step and the infusion step provides exquisite control of the nanocrystal size, morphology, and dispersibility within the pores, without perturbing the morphology of the mesoporous silica.

High loadings of nanocrystals in mesoporous silica over 2 wt % were obtained in carbon dioxide-toluene mixtures in 24 h. It is estimated that roughly 10−100 nanocrystals were infused per pore inside the mesoporous silica. The loadings approached equilibrium and the individual nanocrystals were highly dispersed according to TEM. In contrast, the loadings were small with pure toluene or toluene mixed with the antisolvent methanol. The differences in loadings were correlated with the long-ranged van der Waals forces between gold and silica through the intervening solvent, as described by the Hamaker constant, A_{132}. As CO_2 has an unusually low polarizability/density (very weak vdW forces), it may be added to a liquid solvent to form a mixture with an unusually low Hamaker constant. The weaker vdW forces for the intervening solvent result in a stronger interaction between the gold and silica and a higher chemical potential for the gold in the mixed solvent. Both factors raise the nanocrystal adsorption on the surface and thus the equilibrium loading. Furthermore, the loading may be tuned over a wide range by varying the CO_2 composition. The difference in pore size had only a small effect on the loadings, even when the aspect ratios reached 0.9, indicating pore blockage was minor. Thus it appeared that the adsorbed nanocrystals were mobile, despite the proximity of the nanocrystals to the surface even at the center of a pore.

The simplicity of this infusion method, in that well-known independent syntheses may be utilized for both the nanocrystals and silica, allows for the facile production of nanocrystal/silica composites for applications such as catalysis and optoelectronics. The approach is general and may be applied to the wide varieties of nanocrystals and mesoporous materials that are available or are being discovered.

Acknowledgment. This material is based upon work supported in part by the STC Program of the National Science Foundation under Agreement CHE-9876674, the Department of Energy Office of Basic Energy Sciences, the Robert A. Welch Foundation, and the Separations Research Program at the University of Texas. We are also thankful to Dr. Roger T. Bonnecaze for his help in interpreting the results.

CM051052W

(70) Vigne-Maeder, F.; Amrani, S. E.; Gelin, P. *J. Catal.* **1992**, *134*, 536.
(71) Zhang, Z.; Lagally, M. G. *Science* **1997**, *276*, 377−383.
(72) Fukuoka, A.; Araki, H.; Kimura, J.-i.; Sakamoto, Y.; Higuchi, T.; Sugimoto, N.; Inagaki, S.; Ichikawa, M. *J. Mater. Chem.* **2004**, *14*, 752−756.
(73) Ghosh, A.; Ranjan Patra, C.; Mukherjee, P.; Sastry, M.; Kumar, R. *Microporous Mesoporous Mater.* **2003**, *58*, 201−211.